Empirical Approaches to the Application of Mathematical Techniques in Health Technologies[†]

Anthony G. Shannon[*], Hung T. Nguyen

Faculty of Engineering and Information Technology
University of Technology, Sydney, NSW 2007, Australia
E-mails: Anthony.Shannon@uts.edu.au, Hung.Nguyen@uts.edu.au

[*]*Corresponding author*

Received: July 09, 2013 **Accepted: October 04, 2013**

Published: October 15, 2013

Abstract: *Mathematical modeling of ageing is built in this paper around research and development activities in cooperation with pharmaceutical companies and hospitals. The interaction of "dirty data" with appropriate mathematical techniques is exemplified mainly with applications to health technologies in endocrinology and oncology. The emphasis is more on old techniques in new situations than on new techniques, though there are references to some novel approaches to modeling.*

Keywords: *Diabetes mellitus, Neural nets, Generalized nets.*

Introduction

Ageing populations are a problem for many developed countries this century, both in terms of numbers of "baby boomers" at an economic level and how to help citizens at an individual level [1]. In considering the mathematics of human biology, particularly in relation to ageing, there are two sets of non-communicable diseases which cannot be ignored because they are linked to so many other ailments. These are diabetes mellitus and cancer. Aspects of both are outlined in this paper.

In a clinical sense, as far as we know, these diseases are unrelated. In the context of this paper, their connections are:

- genetically: a cocktail of genes can predispose people to these diseases, together with
- environmentally: aspects of their symptoms and rate of development can be related to life-style,
- through associated factors in the postulated "Metabolic Syndrome *X*", and
- mathematically: neural nets and generalized nets have been used by us in modeling both diseases.

Neither disease is a single entity even at the macro level which is what we shall be considering here. Both provide ample scope for the application of mathematics to medicine, because once one is beyond the basic biochemistry one is into almost the whole of medicine. Moreover, their high incidence correlates well with shifts to the sedentary lifestyles of modern life, a double burden for many parts of the developing world which already suffer from a high prevalence of infectious diseases [2].

[†]An abbreviated version of an invited paper at a London Mathematical Society Conference, Northumberland University, Newcastle-upon-Tyne, UK, 6-8 June, 2012.

Both diseases are replete with dirty data which challenge the medico, the mathematician and the engineer who implements health technology. Not that the mathematical techniques used are necessarily very advanced. The trick is to find what is appropriate for the clinical data in a given situation. Then just as progress seems to be within our grasp new refinements and analyses provide new challenges.

Thus a few years ago when diabetes mellitus (DM) seemed to be understood as two different diseases (Type 1 DM (T1DM) and Type 2 DM (T2DM)) with similar symptoms, epidemiologists began to get new doubts [3]. Now endocrinologists are getting to grips with a number of manifestations of DM, particularly T1.5DM or LADA (Latent Autoimmune Disease in Adults) [4] which is leading to reviews of previous diagnoses [5].

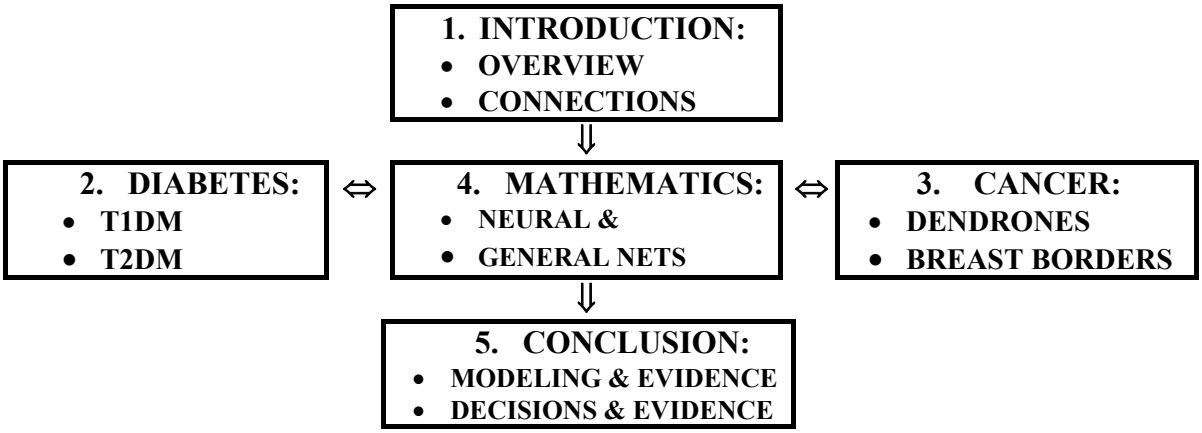

Fig. 1 Plan of paper

Diabetes mellitus

The two key chemicals in the constant endeavour of the body to produce energy are glucose and insulin. The hormone insulin facilitates the entry of glucose into cells for conversion into energy. Diabetes can be a result of the impairment of the ability of the body to obtain the energy it needs to function properly.

T1DM is the name given to that form of the disease where the endogenous production of the insulin in the pancreas is eliminated. Insulin from an external source needs to be provided, usually by subcutaneous (SC) injection [6].

In the case of T2DM it is usually the quantity or efficacy of insulin that is affected, but there is still secretion of insulin from the pancreas. This form of the disease is usually treated with a combination of diet, exercise and oral agents, though sometimes insulin treatment is also required, especially if it is really LADA (Fig. 2).

Essentially, the two forms of diabetes are different diseases with similar symptoms. In both cases, diabetes mellitus is a chronic state of excessive concentration of glucose in the blood. The major regulator of glucose concentration in the blood is insulin, a hormone synthesized and secreted by the beta cells of the islets of Langerhans in the pancreas. High blood sugar levels may be due to a lack of insulin and/or to excess of factors that oppose its action and cause insulin resistance.

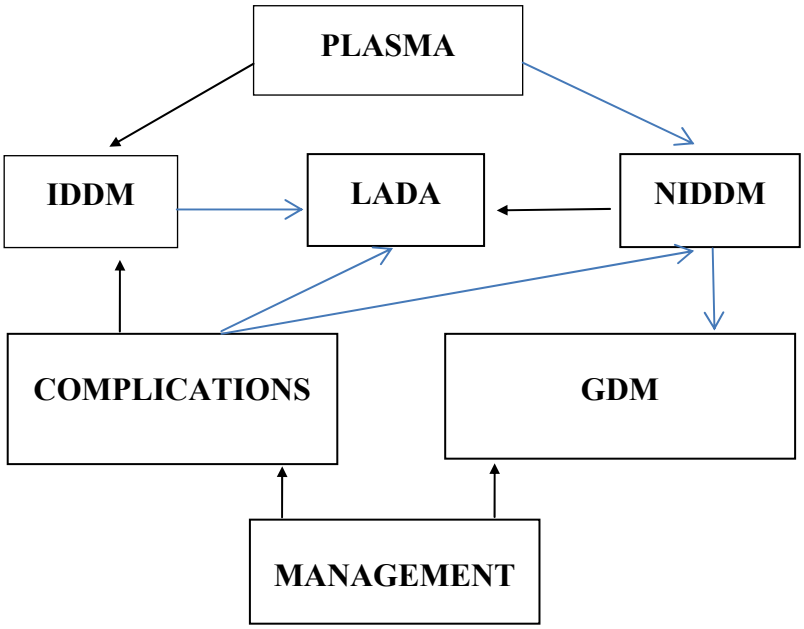

Fig. 2 Aspects of diabetes discussed in the paper

Legend:

- IDDM: Insulin Dependent Diabetes Mellitus (DM1)
- LADA: Latent Auto-immune Disease of Adults (DM1.5)
- NIDDM: Non-insulin Dependent Diabetes Mellitus (DM2)
- GDM: Gestational Diabetes Mellitus

This imbalance can lead to abnormalities of carbohydrate, protein and lipid metabolism. The major complications of diabetes include characteristic symptoms, the progressive development of disease of the capillaries of the kidney and retina, damage to the peripheral nerves, and accelerated arteriosclerosis [7]. There are identifiable stages in the onset of DM2, impaired glucose tolerance and insulin resistance being two of them [8].

Owens [9] presents a historical summary of the disease, and Bliss [10] relates the human drama and scientific enterprise behind the discovery of insulin: "glory enough for all!". We shall focus initially on plasma measurements.

Subcutaneous insulin absorption rates in T1DM

The mathematical modelling of subcutaneous insulin clearance and prehepatic insulin secretion is clinically very useful for several reasons. The process itself is quite complicated and the modeling permits us to focus on the salient features. The process is affected by such factors as insulin concentration, the half-life of the insulin, the site, method and type of injection [11]. Knowledge of insulin kinetics also has uses in the study of pre-diabetes [12] and diabetic complications [13, 14], as well as in such therapeutic innovations as pumps [15], jet injectors [16] and bio-synthetic human insulins [17, 18].

Insulin absorption rates are altered in the diabetic state [19] and this affects the relation between insulin absorption and the resulting plasma insulin concentration [20]. Insulin absorption can be determined experimentally by labeling the insulin with a radioactive tracer such as I^{125}, and then injecting the labeled preparation subcutaneously; the disappearance of radioactivity from the injection site can then be measured.

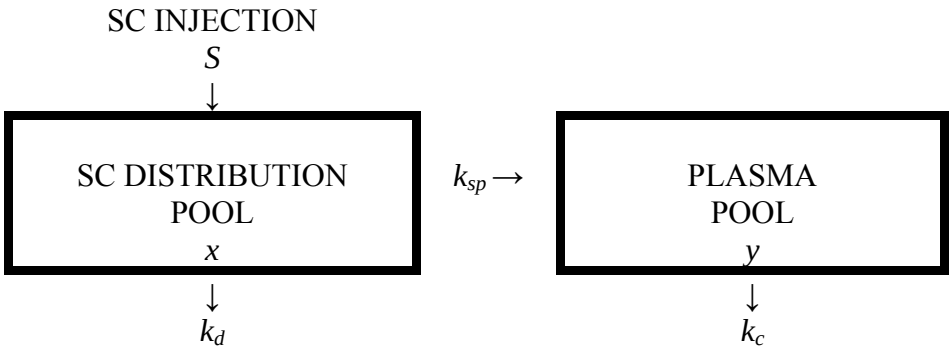

Fig. 3 Compartment model for insulin absorption after a SC injection for patients with T2DM

The amount of radioactivity remaining at the injection site can then be plotted against time to obtain a characteristic curve for each type of insulin which is useful for the physician in planning a regimen of insulin doses and types for individual patients. Studies have shown that I^{125} insulin injected subcutaneously is not normally degraded at the insulin site. It can therefore be assumed that the disappearance of radioactive labeled insulin from the injection site parallels the absorption of the insulin [21].

A theoretical model was postulated with a two-compartment (pool) [22] as schematically represented in Fig. 3. A single pool was envisaged for the SC distribution of insulin following an injection (bolus) of S international units. It is acknowledged that this is an oversimplification of the biological process since it assumes that all SC insulin is immediately available for transcapillary absorption. The model than assumes a fractional rate of systemic delivery k_{sp} and a degradation rate constant k_d from the SC pool. The plasma pool represents the plasma distribution volume with k_c as the metabolic clearance rate.

The mathematical equations which represent the theoretical model are then

$$\frac{dx}{dt} = S\delta(t) - k_d x - k_{sp} x \tag{1}$$

and

$$\frac{dy}{dt} = k_{sp} x - k_c y \tag{2}$$

where x and y are the amounts of SC insulin in pools 1 and 2 respectively, and $\delta(t)$ is defined by

$$\delta(t) = \begin{cases} 1 & if\ t = 0, \\ 0 & if\ t > 0. \end{cases}.$$

The next step is to do something about the parameters. Observation of the appearance of insulin in the plasma shows a rising curve initially [23]. This suggests that insulin is delivered to the plasma pool as

$y \propto t^a\ (a > 0)$ or

$$\frac{dy}{dt} = \frac{ay}{t} = k_{sp}x, \quad (t \neq 0) .$$

Eq. (2) then becomes

$$\frac{dy}{dt} = \frac{ay}{t} - k_c y. \tag{3}$$

While aware of the danger of becoming slaves to a model, there subsequently seemed to be an experimental justification for these assumptions. Disappearance from the SC site is found from

$$\frac{dx}{dt} = -\left(k_d + k_{sp}\right)x = -kx \text{ or}$$

$$x = x_0 e^{-kt} \tag{4}$$

which can be readily linearized. Appearance in the plasma (or clearance from the injection site) is found from Eq. (3), which can be rewritten as

$$\begin{aligned} &\frac{1}{y}\frac{dy}{dt} - \frac{a}{t} = -k_c \\ &\frac{d}{dt}\ln y - a\frac{d}{dt}\ln t = -k_c \\ &\frac{d}{dt}\ln\left(\frac{y}{t^a}\right) = -k_c \\ &y = y_0 t^a e^{-k_c t}. \end{aligned} \tag{5}$$

From Eq. (5) we have that

$$\frac{dy}{dt} = ay_0 t^{a-1} e^{-k_c t} - k_c y_0 t^a e^{-k_c t}$$

the former term on the right hand side of the last equation being the non-degraded clearance rate from the SC site and the latter term being the clearance rate from the plasma pool.

External disappearance of I^{125} labelled human soluble insulin (U100) with simultaneous measurement plasma immunoreactive insulin, C-peptide and glucose was used to study this insulin absorption. To assess the relationship between insulin absorption and subcutaneous blood flow the latter was measured by the disappearance of 99M technetium.

Initial studies consisted of five normal subjects studied on four occasions. On the first three study days insulin absorption was measured from the anterior abdominal wall with simultaneous measurement of subcutaneous blood flow from an injection site adjacent to the insulin injection site. The measurement of SC blood flow from this latter site was compared to a simultaneous injection of technetium on the opposite side of the abdominal wall. On the fourth study day subjects received only insulin. Each study day commenced with three

basal blood samples at -60, -30 and 0 minutes. The six international units of labeled insulin were injected at time 0 minutes, and thereafter blood samples were obtained at 10 minute intervals for the first hour, every 15 minutes for the second hour, and subsequently every half hour until 6 hours after the injection. External disappearance of the insulin and technetium was measured continuously for the first 2 hours and thereafter for 5 minutes at the time of blood sampling.

Six DM subjects were then subjected to the same regime. Their disappearance results are displayed in Table 1, which tabulates the percentage residual activity of the technetium injected adjacent to the insulin injection site over the first 8 minutes.

Table 1. Measured percentage residual radioactivity for 6 subjects during first 8 minutes

Time	Subjects					
(min)	1	2	3	4	5	6
0	100.000	100.000	100.000	100.000	100.000	100.000
1	88.761	89.885	94.262	87.759	92.457	88.265
2	81.613	83.968	85.551	79.320	87.215	78.606
3	72.272	79.510	77.392	71.445	82.852	71.069
4	66.100	72.955	69.424	64.936	78.705	65.968
5	60.142	66.077	64.273	58.378	74.840	60.170
6	53.720	61.891	58.582	52.023	70.523	54.035
7	50.226	59.103	52.886	48.126	66.183	50.549
8	44.617	54.725	47.480	44.693	64.275	45.605

Table 2. Calculated percentage residual radioactivity for 6 subjects during first 8 minutes and the resulting parameter values – fitted to Eq. (4)

Time	Subjects					
(min)	1	2	3	4	5	6
0	98.755	98.125	102.233	97.617	98.259	96.731
1	89.422	91.089	93.036	88.226	93.004	87.992
2	80.971	84.558	84.666	79.738	88.031	79.916
3	73.319	78.494	77.049	72.066	83.323	72.638
4	66.389	72.866	70.117	65.133	78.868	66.023
5	60.115	67.641	63.809	58.867	74.650	60.011
6	54.434	62.791	58.068	53.203	70.658	54.546
7	49.289	58.289	52.844	48.085	66.880	49.579
8	44.631	54.109	48.090	43.459	63.303	45.064
x_0	0.988	0.981	1.022	0.976	0.983	0.970
k	0.099	0.074	0.094	0.101	0.055	0.096
r^2	0.998	0.995	0.998	0.997	0.966	0.966

Some "appearance" results are set out in Table 3. They show the six subjects' plasma insulin concentration (nmol/l) corresponding to the time vector (min) in the left-most column. Thus the ratio of appearance (A) to disappearance (D) has the form

$$\frac{A}{D} = kt^a e^{-bt} \tag{6}$$

which can also be linearized so that multiple linear regression analysis can be used to fit the data.

Table 3. Measured plasma insulin concentration (nmol/l)

Time	Subjects					
(min)	1	2	3	4	5	6
-60	0.042	0.072	0.030	0.036	0.024	0.024
-30	0.030	0.084	0.030	0.024	0.024	0.024
0	0.030	0.060	0.030	0.018	0.030	0.024
10	0.066	0.054	0.048	0.030	0.030	0.030
20	0.120	0.072	0.078	0.042	0.036	0.072
30	0.144	0.108	0.090	0.072	0.048	0.060
40	0.126	0.114	0.090	0.090	0.042	0.090
50	0.150	0.150	0.102	0.090	0.054	0.108
60	0.150	0.120	0.096	0.072	0.054	0.114
75	0.150	0.108	0.072	0.102	0.060	0.102
90	0.132	0.102	0.090	0.102	0.042	0.084
105	0.138	0.096	0.090	0.096	0.054	0.078
120	0.132	0.078	0.090	0.108	0.048	0.078
150	0.114	0.096	0.084	0.090	0.054	0.096
180	0.108	0.102	0.078	0.066	0.036	0.066
210	0.072	0.090	0.054	0.090	0.030	0.054
240	0.054	0.060	0.066	0.054	0.024	0.048
270	0.048	0.054	0.072	0.054	0.030	0.060
300	0.036	0.048	0.048	0.042	0.024	0.036
330	0.024	0.042	0.030	0.042	0.018	0.024
360	0.030	0.030	0.024	0.042	0.030	0.024

The curvilinear relationship (6) was then fitted and the resulting parameters are listed in Table 4.

Prehepatic insulin secretion rates in T2DM

By utilizing the experimental facts that insulin and connecting peptide (C-peptide) are secreted in equimolar amounts from the pancreas [24] and that the C-peptide is not stored in the liver, a non-invasive method of estimating the pre-liver insulin secretion rate was developed [25]. The basic assumption was that there is an "instantaneous" surge of insulin in response to a glucose challenge. In a global sense this is reasonable, though a detailed analysis of insulin concentration profiles sometimes shows a bi-modal, and even occasionally a tri-modal, response curve if the time intervals of measurement are close enough. Previous models have required a guess for the initial value, and this can lead to ill-conditioning problems with multimodal response curves.

It was a conscious decision to opt for the simplest scenario as the starting point for the development of the differential equation, and in most cases it turned out to be an exceptionally good fit, as measured by the coefficient of determination.

The only other assumption was that the rate of clearance of the insulin from the plasma was proportional to the concentration of insulin present in the plasma, a reasonable assumption in the absence of evidence to the contrary and in the light of the results stated later where the insulin kinetics were traced with radioactive markers. We can then use C-peptide levels to

estimate insulin secretion as schematically represented in Fig. 4. This approach was adopted in Cobelli [26] and Vølund [27].

Table 4. Calculated plasma insulin concentration (nmol/l) and appearance/disappearance parameters

Time	Subjects					
(min)	1	2	3	4	5	6
0	2.104	2.118	2.521	2.561	2.820	2.453
10	0.406	0.313	0.299	0.269	0.196	0.291
20	0.274	0.203	0.186	0.164	0.109	0.180
30	0.217	0.159	0.142	0.125	0.079	0.137
40	0.183	0.134	0.118	0.104	0.063	0.113
50	0.160	0.118	0.102	0.091	0.054	0.098
60	0.143	0.106	0.091	0.082	0.047	0.087
75	0.124	0.094	0.080	0.073	0.041	0.076
90	0.110	0.085	0.073	0.067	0.037	0.068
105	0.099	0.079	0.067	0.063	0.034	0.063
120	0.090	0.074	0.063	0.060	0.032	0.058
150	0.076	0.066	0.057	0.056	0.029	0.052
180	0.066	0.062	0.053	0.054	0.028	0.048
210	0.058	0.058	0.050	0.053	0.027	0.045
240	0.052	0.055	0.048	0.053	0.027	0.043
270	0.047	0.054	0.047	0.054	0.028	0.041
300	0.042	0.052	0.046	0.056	0.028	0.040
330	0.038	0.051	0.046	0.058	0.029	0.039
360	0.035	0.050	0.046	0.060	0.030	0.038
k	0.380	0.324	0.404	0.434	0.427	0.433
a	-0.545	-0.646	-0.718	-0.763	-0.903	-0.716
b	-0.098	-0.076	-0.096	-0.105	-0.059	-0.097
r^2	0.989	0.986	0.987	0.987	0.958	0.985

The main purpose of this part of the study was to determine whether as fasting plasma glucose levels increased the insulin secretion rate decreased in response to a carbohydrate challenge and also whether obese subjects had a lower insulin secretion rate than non-obese subjects.

Suppose $R(t)$ is the rate of secretion from the pancreas into the portal vein of both the insulin and the C-peptide in Fig. 4, and $(1 - F)$ is the unknown fractional uptake of insulin by the liver. To accommodate the initial response by the pancreas to a glucose load, we assumed the rate of secretion of each peptide is directly proportional to the concentration in the plasma and inversely proportional to time with respective coefficients of proportionality a_I and a_C. This is a pragmatic assumption based on experimental observations of results where the glucose challenge is derived from oral glucose tolerance tests (OGTT) and meal tolerance tests (MTT):

$$\frac{dC}{dt} \propto \frac{C}{t}.$$

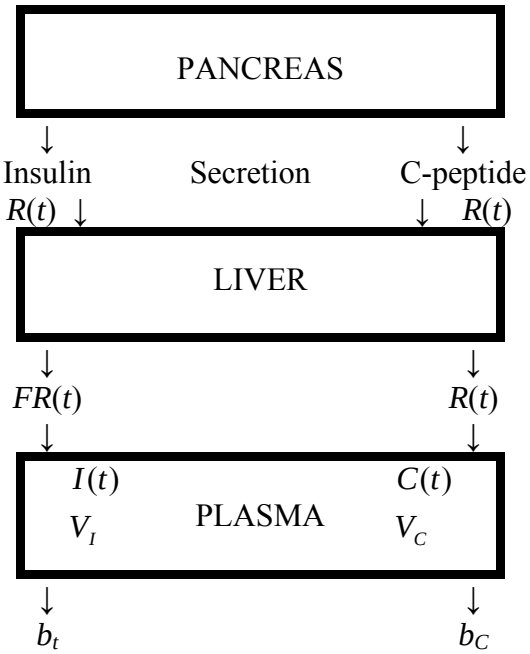

Fig. 4 Compartment model of peptide secretion for T2DM

This assumption was originally prompted by work on the two-pool model for insulin secretion. In this, one pool is conceived as a small compartment available for rapid insulin release, and the other for sustained insulin release [28]. Beyond that the use of the assumption leads to consistent results as we shall see. In any case, the hypothesized multiphasic close temporal associations between pulses of insulin secretion and blood glucose levels are the object of considerable debate [29].

We seek $R(t) = dC / dt$. The C-peptide kinetics can then be described by the first order differential equation

$$\frac{dC}{dt} = a_C \frac{C}{t} - b_C C \tag{7}$$

a solution of which is

$$C = C_0 + At^{a_C} e^{-b_C t} \tag{8}$$

in which A is a scaling factor.

If we differentiate Eq. (8) we obtain

$$\frac{dC}{dt} = Aa_C t^{a_C - 1} e^{-b_C t} - Ab_C t^{a_C} e^{-b_C t} \tag{9}$$

which is consistent with Eq. (6) as we would expect. The first term on the right hand side of Eq. (9) is the secretion term and the second term is the clearance term.

In the following experimental studies all subjects were given an MTT after a 10 hour overnight fast. The meal used is summarized in Table 5. The subjects were allowed 10 minutes to consume the meal.

Table 5. Composition of MTT [30] (A: Made up to 200 ml volume with water)

Food	Amt (g)	Energy (kcal)	Protein (g)	Fat (g)	Total CHO (g)	Sugars (g)	Starch+ dextrins (g)	Diet fibre
Weetbix	15	51.0	1.71	0.51	10.55	0.92	9.98	1.90
Skimmed milk powder[a]	10	35.5	3.64	0.13	5.28	5.28	0	0
Pineapple juice	250	132.5	1.00	0.25	33.50	33.50	Trace	0
White meat chicken	50	71.0	13.25	2.00	0	0	0	0
Hovis bread	60	136.8	5.82	1.32	27.06	1.44	25.62	2.70
Butter	9	66.6	0.04	7.38	Trace	Trace	0	0
Totals		493.4	25.46	11.59	76.39	41.14	35.60	4.60
%Calories		100	20	20	60			

As a pilot study we investigated 11 T2DM subjects and 7 non-diabetic subjects. The slope is from y_0 to y_{max} when the clearance action is first perceived. After the overnight fast, the subjects were admitted to a metabolic unit, where they remained on bed rest throughout the study; smoking was not permitted. Mixed venous blood samples were taken from a forearm vein at 08.30 h and immediately prior to the administration of the MTT at 09.00 h, and then at 30 minute intervals for 4 hours.

The C-peptide data were then fitted using multiple linear regression of Y on x and t. Table 6 shows the values of the parameters for the 11 diabetic and 7 non-diabetic subjects in the pilot study following the MTT.

The average results are shown in Table 7 following this MTT. The most obvious difference between the two groups is, not surprisingly, in the slope, though this is really a side-issue in the present study, particularly in the pilot study. However, it does illustrate that the model picks up the sharper response of the non-diabetic subjects to the glucose load.

As an example of the goodness-of-fit, the measured (m) and the calculated (c) C-peptide levels for the T2DM subjects 1 and 6 are shown in Table 8. A statistical analysis of the issues in goodness-of-fit is discussed in some detail in [31].

The pilot study was carried out at the Prince of Wales Hospital in Sydney, Australia. The main study, which followed, was performed at the University Hospital in Cardiff, Wales, after the model was discussed with researchers from the Radcliffe Infirmary in Oxford, England, where Marie Shannon, who had brittle T1DM, was a patient. In this study there were 235 T2DM patients. All patients had normal kidney and liver function tests, though as an indication of glycaemic control the glycosylated haemoglobin (HbA1) concentration of the patients varied from 6.7 to 19.3% (mean 11.6, SD 2.5%). (For comparison, a normal range is 5.5-7.8%). The DM subjects were also sub-divided into three subgroups labelled, “mild”, “moderate” and “severe”. For other later clinical work too, as well as to test the model, the patients were also divided into obese and non-obese subgroups according to body mass index

(BMI = body mass/height^2). It was used because it partly accounts for the distribution of the body mass. A BMI < 26.5 kg/m^2 was considered as non-obese here. In addition, 56 normal subjects of similar age range and no family history of DM were studied.

Table 6. Individual subjects in pilot study

T2DMs	*a*	*b*	r^2	slope
1	1.412	0.008	0.94	0.001
2	8.027	0.075	0.92	0.001
3	2.523	0.021	0.93	0.001
4	2.080	0.026	0.93	0.001
5	1.789	0.024	0.73	0.009
6	4.711	0.105	0.60	0.004
7	8.770	0.067	0.82	0.014
8	8.630	0.086	0.87	0.002
9	9.104	0.089	0.89	0.004
10	3.519	0.036	0.94	0.007
11	2.395	0.026	0.95	0.006
Non-DMs	*a*	*b*	r^2	slope
1	1.590	0.024	0.78	0.014
2	3.210	0.058	0.98	0.026
3	3.791	0.047	0.94	0.019
4	2.561	0.032	0.90	0.020
5	11.533	0.120	0.91	0.061
6	1.938	0.118	0.95	0.024
7	3.780	0.045	0.96	0.022

Table 7. Pilot study parameters for Eq. (7)

Subjects	*N*	a_C	b_C	r^2	slope
T2DM	11	4.815	0.052	0.87	0.005
Non-DM	7	4.058	0.063	0.92	0.027

Table 8. Comparisons at specific sampling times for T2DMs 1 and 6

	time (min)	0	15	30	45	60	75	90	120	150	180
#1	*m*	0.11	0.14	0.18	0.19	0.24	0.26	0.37	0.43	0.39	0.34
	c	0.11	0.14	0.17	0.21	0.25	0.27	0.30	0.33	0.35	0.36
#6	*m*	0.37	0.45	0.48	0.52	0.42	0.42	0.41	0.39	0.41	0.24
	c	0.37	0.39	0.39	0.38	0.37	0.37	0.37	0.37	0.37	0.37

Cancer

In this section a simple means of determining the breast region from an image dendrogram is described. The goal is to improve the delineation in mammograms to improve their reading by radiologists and so reduce the error rates (both false-positives and false-negatives).

A dendrogram is a combinatorial tree diagram to analyse the arrangements in hierarchical clustering. Essentially, the method here, which is an improvement on Mitchell [32], entails choosing one of the dendrones, or branches of the image dendrogram, and marking it as the breast area.

According to Hanusse [33], the hierarchical and automated fashion in which the image dendrogram is created, leads to a meaningful depiction of the semantic information that "explains" the image, and exhibits the objects it contains, along with their relationships. Thus, various observations can be seen from the structure of the dendronic representation of the image. In Fig. 5, an image and its corresponding dendrogram can be seen.

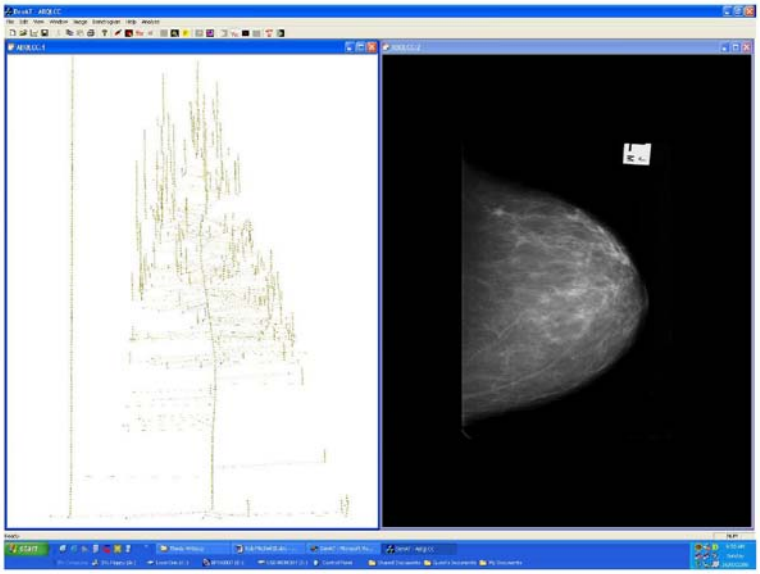

Fig. 5 Mammogram (right) and corresponding dendrogram (left)

In the image, our human vision system instantly recognizes that there are two main objects present: one lead marker that is relatively uniform, and the other, a breast that is comprised of other objects and tissues within it. A partial description of this can be seen in the dendrogram in which there are two main branches: one long "skinny" branch that corresponds to the lead marker, and another, "bushy" branch that corresponds to the breast. The latter is comprised of other sub-branches or objects, hence its "bushy" appearance. The effectiveness of the dendrogram enables us to discriminate between branches or objects in the image.

Utilizing the dendrogram as a structural description of the image, both the breast and lead marker branches can be found. Once they are found, all other extraneous objects can be discarded, as they represent only noise or other unwanted artefacts in the background. Given the breast branch of the dendrogram, the border can be shown, and the region in which to search for cancer is therefore also known. This is the first stage in the analysis of the created dendrogram.

In detecting the breast and lead marker branches within the dendrogram, two values are tested for the branches within it. Using these two values, coined here as Dendrone Slenderness Ratio and Border Gradient, a scheme utilizing simple thresholds has been developed to discriminate between the breast and lead marker branches from the dendrogram, and thus their corresponding regions within the image.

Dendrone Slenderness Ratio

Consider the two dendrones in Fig. 6 where it can be seen that the first dendrone (a) depicts one main branch, or object, and appears to be rather "skinny". The other dendrone (b) consists of one gross object containing two sub-objects, and appears to be more "bushy".

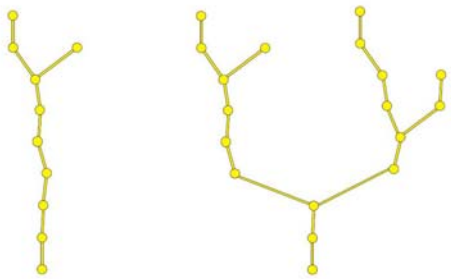

a) b)

Fig. 6 Two examples of dendrones: a "skinny" one (a), and a "bushy" one (b)

The description of these dendrones is similar to that of the description of a lead marker dendrone and a breast dendrone, respectively. One way in which this description can be interpreted by the dendrone is its value of the Slenderness Ratio. The Slenderness Ratio gives the value of how "skinny" a branch is. A branch that is one persistent branch has a value of 1, and more "bushy" branches have a value less than unity. The Slenderness Ratio is defined numerically by:

$$SR = \frac{L_{\max}}{N_c}$$

in which $L_{\max}$ = maximum length of the dendrome and N_c = total number of clusters in the dendrome. For the dendrones in Fig. 6, both have a maximum length of 9 and total numbers of clusters are 10 and 18 respectively. This gives the "skinny" dendrone (a) a Slenderness Ratio of 0.9, while the "bushy" dendrone (b) has a Slenderness Ratio of 0.5.

It was found that dendrone branches representing the breast regions of the image had very low values for Slenderness Ratio. Likewise, dendrones which correspond to the uniform lead marker in the images had very high Slenderness Ratios. In the search for the breast and lead marker dendrones, the thresholds of Slenderness Ratio used in their detection were found to be 0.4 and 0.7, respectively.

Thus, the image dendrogram could be very quickly searched, from the lowest level first, to see which branches corresponded to breast or lead marker Slenderness Ratios. While the Slenderness Ratio alone gave the correct branches for the breast and marker in the images, it was not sufficient in selecting the optimum cluster. Thus, another discriminator was needed. Initially, shape descriptors such as elongation and area ratio were used as this supplement. Subsequently, however, one single descriptor, average Border Gradient was found to be faster and more effective as an extra descriptor.

Average Border Gradient

Traditional image processing techniques used in object detection include Edge Enhancement/Detection. They are commonly implemented through spatial filters, such as Shift and Difference, Prewitt Gradient, Laplacian and Sobel operators. Their output produces borders based on gradients and can be used in subsequent image analysis operations for feature or object recognition.

In the case for breast detection using the dendronic representation of the image, the process is somewhat reversed. The dendronic structure corresponds to the objects within the image, and

this implies that the borders of each of those objects are also known. Thus, the border of a given object can be tested to see if it corresponds to that of the type being detected.

Accordingly, a modified border gradient operator has been devised and applied to the dendronic representations of the mammograms in order to obtain the average gradient along the border of each candidate breast or lead marker branch. As with other spatial pixel group operators, the modified gradientoperator relies on a marching template, but it does not operate on the whole image, rather just the pixels on the border of the object of interest. The template for the operation can be seen in Fig. 7.

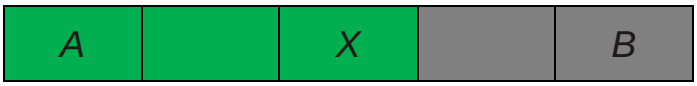

Fig. 7 Template for Border Gradient calculation

Here, the pixel *X* is the pixel on the border between the object (colour green) and the surrounding area (colour grey). In order to obtain the average pixel gradient at pixel *X*, the following expression is evaluated:

$$G_X = \frac{I_A - I_B}{4}$$

in which I_A and I_B are the pixel intensities at *A* and *B*, respectively.

Once the gradient at each border pixel is found, the average Border Gradient is calculated. This value is then used to evaluate if the branch in question is the breast branch or not. It was found that threshold values for the breast Border Gradient were much less than the threshold for the lead marker. This is to be expected, as the lead marker possesses a very well defined edge. A value of $G_X = 0.4$ gave a suitable threshold for deciding whether or not the object in question was the breast region, while a value of $G_X = 1.0$ gave a suitable threshold for deciding whether or not the object in question was the lead marker.

It should be noted that this simple method only calculates the border gradient in one direction, along the horizontal. However, as a majority of the breast border is in a vertical direction, this simple method captures the gradient across the breast border well, and helps to discriminate it from other objects in a robust fashion.

Breast border detection process

In order to arrive at the threshold values for both the Slenderness Ratio and Border Gradient, four mammograms were chosen randomly from the full dataset. These comprised two craniocaudal and two mediolateral oblique mammograms. From these images, the threshold values required to identify the breast and marker dendrone were found. A factor was applied to the most marginal threshold values in order for them to be more universal.

It is assumed that the breast region is of a higher intensity than that of the background. Thus, the dendrogram is scanned commencing with the cluster(s) in the lowest intensity level. In this way, the lowest intensity outer contour of the breast region will be found. Should the breast branch not be found in the first level or two, detection will continue for higher intensities, and breast contours of higher intensities would be found, these corresponding to smaller radius contours as the breast thickness rapidly increases [34].

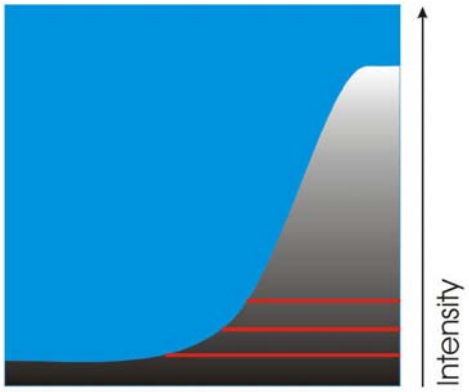

Fig. 8 Exaggerated breast border profile of intensity

It is desirable, however, to stop detection when the lowest intensity border is encountered, as this represents the edge between the breast and the background. In Fig. 8, three contours in the vicinity of the breast border are depicted, each at a different intensity level. Three contours of the breast are shown in red at the bottom of the picture. The gradient of the border at each of the contours increases as the intensity increases. A cluster in the dendrogram will represent each of these contours. Starting with the lower intensity cluster, the border gradient is evaluated and if the Slenderness Ratio is less than 0.4 and the gradient is greater than 0.4, the cluster is labelled as the breast cluster. If not, the next intensity higher is tested.

As can also be seen in Fig. 8, the gradient increases as the intensity increases, near the breast boundary. At some point close to the border, the gradient threshold will be overcome and the breast region will be detected. It has been identified that generation of false alarms, such as lead markers should be avoided so as to prevent the radiologist losing confidence in the algorithm's performance. Therefore, whilst the breast border identification process is underway, the lead marker is also identified. Since Slenderness Ratio is calculated for the objects in the dendrogram, this does not produce a large overhead in performance.

Identification of the marker did not seem necessary using the algorithm developed in the current research, as no marker objects were identified as masses. However, some cases do arise whereby the lead marker overlaps the breast region and may be included as such. Therefore, by identifying the lead marker, it may be excluded from the subsequent mass detection algorithm. In this way, the possibility of a future false alarm caused by detection of the marker as a malignant mass is removed.

The effectiveness of the slenderness ratio, coupled with the average border gradient can be seen in Fig. 9. The use of a Slenderness ratio threshold alone has identified clusters representing the breast and marker – (a) and (c). However, it has not made ideal selections, as there exist background artefacts attached to the objects. By using a threshold on the average border gradient as well, the next appropriate clusters are selected, and they correspond to visually better object representations – (b) and (d).

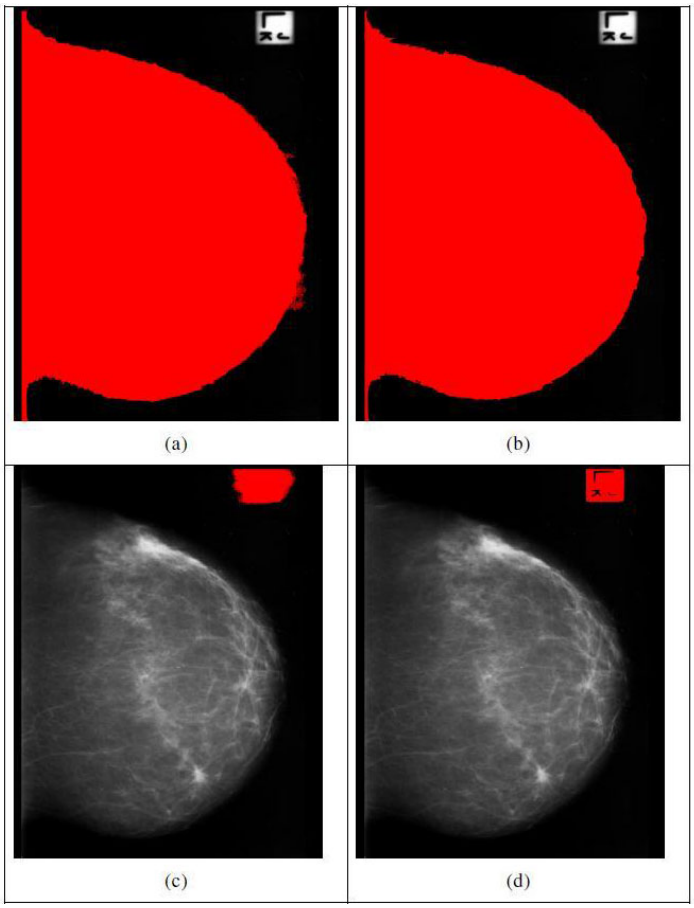

Fig. 9 Breast and marker detection comparison: Using Slenderness Ration alone – (a) and (c) – using Slenderness Ratio as well as Average Border Gradient – (b) and (d).

The breast border detection routine is summarized in the following sequence:

For intensity levels (starting at the lowest intensity):
    For every cluster in the level:
        • Obtain the dendrone's Slenderness Ratio
        • Get the border pixels of the object
        • Get the Average Border Gradient of the object
        If Slenderness Ratio < 0.4 AND Average Border Gradient > 0.4
            → Cluster is the breast region
        If Slenderness Ratio > 0.7 AND Average Border Gradient > 1.0
            → Cluster is the lead marker
        If breast region and lead marker have been found _Finish
    END
END

The test set used to evaluate these threshold values and thus the breast area detection performance, was the remaining 46 mammograms in the data base. The following figures (Figs. 10-13) display a variety of examples of detected lead marker and breast regions. In each sequence,

a) shows the detected breast in green. Other objects in the image have been discarded, so that there are only the two detected objects present.

b) simply shows the detected breast border overlaid on the original image. The breast boundary is found simply from the interface between the green region and the background in (a).
c) shows the original image with an overlaid tracing of the breast border by an expert radiologist, for comparison.

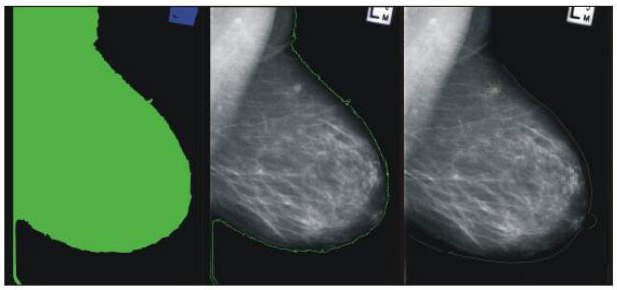

a) b) c)
Fig. 10 ABULCC (ABU – patient code, then L: left, CC (cranio-caudal) view) border etection

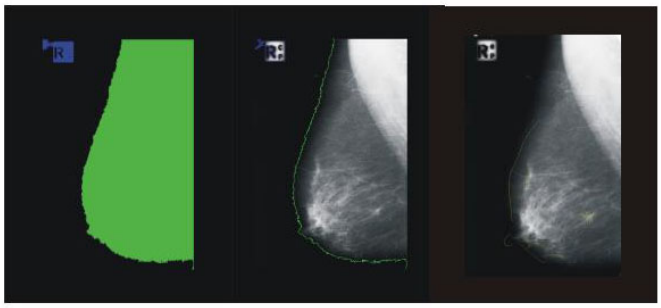

a) b) c)
Fig. 11 ABRRML (ABR – patient code, R: right, ML (mediolateral-oblique) view) border detection

The Slenderness Ratio, while being a robust parameter in the detection of abreast branch, did not always select the optimum cluster in the branch to represent the breast region. Another parameter, the average Border Gradient, which is a pixel level feature of the border pixels of and object, was also utilized to refine the decision. In this way, detection of the breast and marker dendronic branches was achieved.

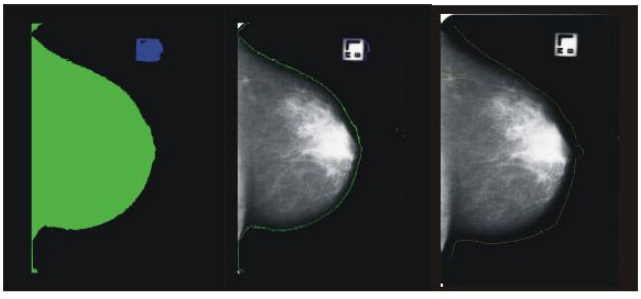

a) b) c)
Fig. 12 ABWLCC (ABW – patient code, then L: left, CC (cranio-caudal) view) border etection

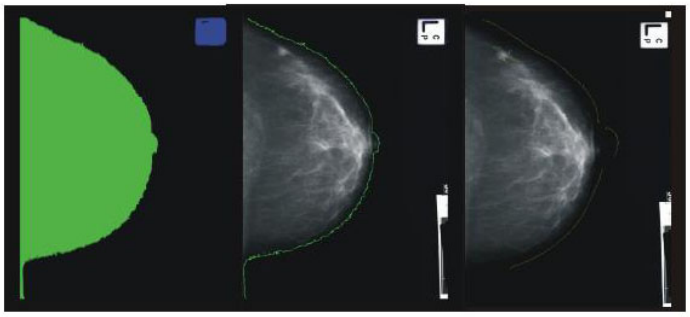

a) b) c)

Fig. 13 ADBRML (ADB – patient code, R: right, ML (mediolateral-oblique) view) border detection

The breast detection method was found to produce a general border that agrees well with a visual inspection of the image. It is also robust to noise and other image artifacts that are of little relevance to the breast region itself. However, when compared to the radiologist's border outline, it can be seen that the detection method does not agree precisely with the shape of the outlined breast. Two further examples of detected breast regions are shown in Fig. 14, together with the radiologist's outlines.

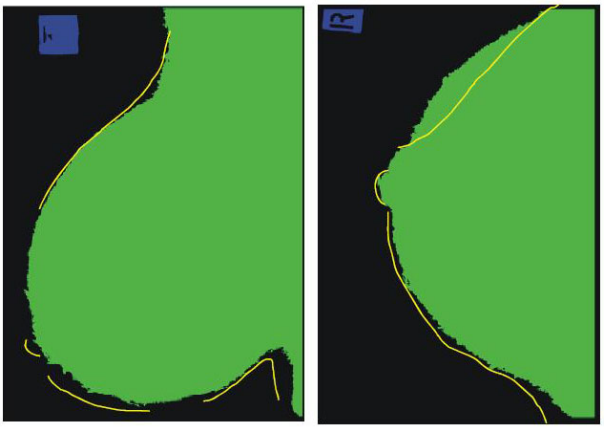

a) b)

Fig. 14 Two examples of detected breast regions. A typical example (a) and an example of a mismatch in shape (b).

In Fig. 14(a), a typical detected breast region agrees fairly well with the radiologist's outlining, but conversely in (b), the shape detected by the method disagrees with the radiologist's outline. It is the authors' opinion that the border detected by the algorithm is closer to the actual borderline of the skin. This assertion can be explained by the method by which the outlines were obtained; it is not to take away from the experience or expertise of the radiologist. Rather, the outlines were obtained with the use of a tablet personal computer. It takes some time to become accustomed to the nuances of the pointing device, particularly in accounting for the pen pressure required. Therefore even with an expert radiologist, the accuracy is dependent on the experience of the radiologist with the technology.

Furthermore, for the display of the digital image being traced, no brightness and/or contrast controls were available, making the job of the radiologist even harder. Another factor to take into consideration is that the outlines should be continuous outlines, rather than broken segments. With the broken outlines of the radiologists as displayed in this research the exact accuracy of the border detection is difficult to quantify at this stage.

Moreover, the roughness of the curve does not correlate well with the smoothness of the real skin border. Other research in breast border detection provides methods for smoothing and obtaining border locations. However, the regions detected using this method envelop the breast area more than adequately for the detection of stellates within the breast. Further, as the complete stellate detection process is essentially automated, this method for breast detection provides a necessary robust framework for subsequent analysis. It is the automated and robust qualities of the dendronic analysis that are of significance.

Other methods will be able to achieve the same breast border, and perhaps be slightly smoother and marginally more accurate, but they are subject to variability in image contrast and other image variables and may not obtain a very good border representation, whereas, the significance of the structure represented by the image dendrogram leads to the detection of the breast sub-structure extremely robustly.

As the test set comprised the remaining, unseen images in the database, the percentage of images used to derive the threshold values was very low at only 8% of the total images. The database of 50 images used in this research was sourced from two large breast screening clinics in a major western city. Therefore, it is expected that the threshold values would apply to mammograms from a similar source and digitized on the same equipment.

Should dendronic image analysis become combined with other mass detection algorithms in the future, a more accurate border detection method might be needed. In many mass detection algorithms, an accurate breast border detection method is required to avoid inaccurate results caused by kernels overlapping the background, for the analysis of architectural distortions or to warp corresponding images taken from other screenings of the same patient [35]. In such cases, a pre-processing step might be implemented, or a more accurate edge detection integrated. The emphasis of the research presented here has been on the applicability of dendronic image analysis in the detection of stellates, and thus pre-processing has been omitted in order to evaluate the effectiveness of raw dendronic analysis alone.

Mathematics

In the work on diabetes in the last section and the work on cancer in the next section, extensive use has been made of generalized nets (GNs) in the former and neural nets in the latter.

As an illustration of the lesser known GNs, we apply them to one aspect of the management of diabetes. GNs are generalizations of Petri and other nets, but their theoretical extensions enable GNs to be applied in a wide variety of applications [36]. This is because GNs can accommodate

- the description of time parameters;
- the logical constraints;
- the capacities of the separate components, and
- the history of the previous cycles of the model.

This means, that like other nets, they are self-learning entities which can be utilized in a wide range of modelling since GNs are modified on the basis of the difference between expected and observed data in relation to certain fixed criteria.

Briefly, a GN is an ordered four-tuple which is combinatorially a di-graph and which

- contains a set of transitions (which, in turn, is described by a seven-tuple);
- a function which prioritises the transitions;

- a function which prioritises the places within the GN;
- a function which prioritises the capacities of the places;
- a function which calculates the truth values of the predicates of the conditions in the transitions – this can utilize "intuitionstic fuzzy logic" [37];
- a function which calculates the next time-moment when a given transition can be activated;
- a function which gives the duration of the activity of any transition;
- a set of tokens which move around the net.

Successful management of diabetes mellitus requires adequate control of blood glucose levels. Hypoglycaemia refers to the situation where there is less than the normal amount of glucose in the blood, usually caused by administration of too much insulin, excessive secretion of insulin by the islet cells of the pancreas or excessive exercise. Some unexplained hypos' happen for no obvious reason and some occur without prior warning signals (asymptomatic). On the other hand, glucagon is a hormone produced in the alpha cells of pancreatic islets of Langerhans. It causes the breakdown of glycogen into glucose thus preventing blood sugar from falling too low in normal circumstance. Hence glucagon prevents hypoglycaemia by maintaining glucose production at a rate sufficient to meet the needs of the human body. A dangerous situation arises when a patient has a series of "hypos" without giving the liver a chance to replenish its supply of glycogen.

However, among diabetic patients when uncontrolled insulin release has been reported (insulin shock), and if the release of glycogen from the liver is not sufficient to counteract the effect of the consequence of the insulin excess, hypoglycaemia will occur. The effect may vary from mild episodes, to severe and intractable hypoglycaemia leading to convulsions and even death in some cases.

We develop a GN which is effectively a directed graph of Fig. 4 above. It is represented in Fig. 15 below.

We let TIME represent the current-time-moment and for a token p, we denote by x_0^p and x_{cu}^p the initial and the current characteristics of the token p:

- α-tokens enter places l_1 with initial characteristics "receiving of signals by the pancreas to begin functioning",
- β-tokens enter place l_4 with initial characteristics: "x_0^b = manufactured insulin; its quantity; the current time-moment"; and
- γ-tokens enter place l_9 with initial characteristic: "x_0^c = carbohydrate; its quantity; the food's type; its quantity; the current time-moment + the necessary time for digestion".

Fig. 15 represents a GN model for diabetes mellitus. The forms of the GN-transitions are the following:

$$z_1 = \langle \{l_1\}, \{l_2, l_3\}, r_1, \wedge(l_1) \rangle$$

$r_1 =$

	l_2	l_3
l_1	true	true

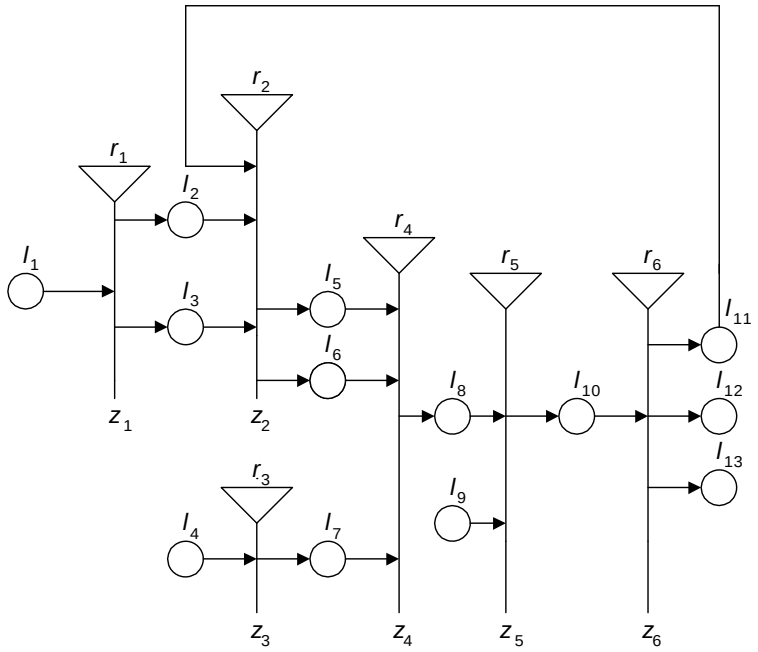

Fig. 15 GN Model for diabetes mellitus

The tokens from place l_2 receive the characteristic "insulin; its quantity; the current time-moment". The tokens from l_3 receive the characteristic "C-peptide; its quantity; the current time-moment".

$$z_2 = \left\langle \{l_2, l_3, l_{11}\}, \{l_5, l_6\}, r_2, \vee\left(\wedge(l_2, l_3), l_{10}\right)\right\rangle,$$

$r_2 =$

	l_5	l_6
l_2	$W_{2,5}$	$W_{2,6}$
l_3	$W_{3,5}$	$W_{3,6}$
l_{11}	true	true

where

- $W_{2,5}$ = "plasma glucose levels are too low";
- $W_{2,6}$ = "plasma glucose levels are too high";
- $W_{3,5}$ = "$TIME - pr_3 x_1^a \geq C_1$";
- $W_{3,6}$ = "$TIME - pr_3 x_1^a \geq C_2$",

in which C_1 and C_2 are insulin time administration constants: $5 \leq C_1, C_2 \leq 15\,\text{min}$ (which vary between different patients and within the same patient from day to day).

The tokens from places l_2 and l_3 are united and then split again and enter the places l_5 and l_6 according to their characteristics l_5: activation of liver's store of glycogen, and l_6: insulin; its quantity; the current time-moment.

$$z_3 = \left\langle \{l_4\}, \{l_7\}, r_3, \wedge(l_4)\right\rangle,$$

$r_3 =$

	l_7
l_4	$W_{4,7}$

where

- $W_{4,7} =$ "$TIME - pr_3 x_1^a \geq C_1$".

The tokens from place l_7 receive the characteristic: "insulin; its quantity; the current time-moment".

$$z_4 = \left\langle \{l_5, l_6, l_7\}, \{l_8\}, r_4, \vee\left(\wedge(l_5, l_6), l_7\right)\right\rangle,$$

$r_4 =$

	l_8
l_5	$W_{5,8}$
l_6	$W_{6,8}$
l_7	$W_{7,8}$

where

- $W_{5,8} = W_{6,8} =$ "$TIME - pr_3 x_{cu}^a \geq C_3$",
- $W_{7,8} =$ "$TIME - pr_3 x_1^b \geq C_3$",

in which C_3 is a constant for which $10 \leq C_3 \leq 30$ min, with variations again between and within patients.

In place l_8 the α-tokens and β-tokens from place l_6 and l_7 respectively are united in one α-token with the characteristic: "insulin; its quantity; glucose; its quantity; there is/there is not hypoglycaemia; the current time-moment".

$$z_5 = \left\langle \{l_8, l_9\}, \{l_{10}\}, r_5, \vee\left(l_8, l_9\right)\right\rangle,$$

$r_5 =$

	l_{10}
l_8	true
l_9	$W_{9,10}$

where

- $W_{9,10} =$ "$TIME - pr_3 x_0^c \geq 0$".

In place l_{10} the α-tokens and the γ-tokens from l_8 and l_9 respectively, are united in one α-token with the previous token's characteristic (place l_8 "insulin; its quantity; the current time-moment").

$$z_6 = \left\langle \{l_{10}\}, \{l_{11}, l_{12,}, l_{13}\}, r_6, \wedge\left(l_{10}\right)\right\rangle,$$

$r_6 =$

	l_{11}	l_{12}	l_{13}
l_{10}	$W_{10,11}$	$W_{10,12}$	$W_{10,13}$

where

- $W_{10,11} =$ "$pr_2 x_{cu}^a \geq C_4$" and "$pr_4 x_{cu}^a \geq C_5$",
- $W_{10,12} =$ "$pr_2 x_{cu}^a \geq C_4$",
- $W_{10,13} =$ "$pr_4 x_{cu}^a \geq C_5$".

The α-tokens from place l_{10} go to one of the places l_{11}, l_{12} and l_{13}, where they receive, respectively, the following characteristics:

- in place l_{11}: " $pr_1 x_{cu}^a$; $pr_2 x_{cu}^a$; $pr_5 x_{cu}^a$ ";
- in place l_{12}: "it is necessary to add insulin";
- in place l_{13}: "it is necessary to add glucose".

More specific details may be found in Shannon et al. [38].

Health technologies related to this research include Intelligent Hand-held Terminals for dietary information [39], Insulin Dosage Meters [40], and HypoMon®, a device for detecting nocturnal hypoglycaemia [41].

Concluding comments

There are other issues for the mathematician in medicine. Difference equations are often, but not always, useful in dealing with data measured at discrete time points [42, 43]. There are also temptations to use techniques more sophisticated than are warranted by the data or to utilize too much data, ignoring the many self-correcting mechanisms in the living body.

This excursion through some aspects of these diseases has not had time to engage with controversies. For instance, is there really such a thing as "brittle" T1DM? are "impaired glucose tolerance" and "insulin resistance" recognizable defined stages in the onset of T2DM? What is the place of "insulin sensitivity"?

There is also the difficulty in deciding what constitutes clinically compelling evidence; after all, not all human issues of life and death lend themselves to the scrutiny of Level 1 evidence: randomized, double-blind, cross-over trials [44].

Acknowledgements

Some of the material here arose from previous work in our supervision of current and former doctoral students, particularly Choy Yee Hung[1] and Robert Mitchell[2]. Patient data were supplied within University and Hospital Human Research Ethics guidelines at different times by:

- *Professor Stephen Colagiuri, Faculty of Medicine, The University of Sydney;*
- *Dr John J Miller, Novo Nordisk Australasia, Baulkham Hills, NSW;*
- *Professor David R Owens CBE, University Hospital Llandough, Cardiff;*
- *Dr Mary Rickard, the New South Wales State Breast Screen Coordination Unit.*

References

1. Henry B. (2007). Modelling Australia's Ageing Population, Parabola, 43(3), 1-8.
2. Heilbuth B. (2011). Double Burden, Development Asia, 4(9), 16-20.
3. Zimmet P., R. Turner, D. McCarthy, M. Rowley, I. Mackay (1999). Crucial Points at Diagnosis: Type 2 Diabetes or Slow Type 1 Diabetes, Diabetes Care, 22(2), 59-64.
4. Tica V., M. W. Hanif, A. Andersson, G. Valsamakis, A. H. Barnett, S. Kumar, C. B. Sanjeevi (2003). Frequency of Latent Autoimmune Disease in Adults in Asian Patients Diagnosed as Type 2 Diabetes in Birmingham, United Kingdom, In Snjeevi C.

[1] Choy Yee Hung (2002). Risk Factors Associated with Renal Disease in Diabetes Mellitus, Unpublished Ph.D. Thesis, University of Technology, Sydney.

[2] Mitchell R. (2006). Efficient Dendronic Creation, Visualisation and Analysis for the Detection of Stellates in Digitised Mammograms, Unpublished Ph.D. Thesis, University of Technology, Sydney.

B., G. S. Eisenbarth, Immunology of Diabetes II: Pathogenesis from Mouse to Man, New York Academy of Sciences, Annals 1005, 356-358.
5. Leslie D., C. Valeri (2003). Latent Autoimmune Disease in Adults (LADA), Diabetes Voice, 48(4), 14-16.
6. Binder, C. (1969). Absorption of Injected Insulin, Acta Pharmacol Toxicol., 27(2), 1-84.
7. Expert Committee on Diabetes Mellitus (1980). Technical Report No. 646, World Health Organization, Geneva.
8. Hansen B. C., J. Saye, L. P. Wennogle (1999). The Metabolic Syndrome *X*: Convergence of Insulin Resistance, Glucose Intolerance, Hypertension, Obesity, and Dyslipidemias – Searching for the Underlying Defects, New York Academy of Sciences, Annals 892, ix-x.
9. Owens D. R. (1986). Human Insulin, MTP Press, Lancaster.
10. Bliss M. (1982). The Discovery of Insulin, The University of Chicago Press, Chicago.
11. Galloway J. A., C. T. Spradklin, R. L. Nelsom, J. M. Warner (1981). Factors Influencing the Absorption, Serum Insulin Concentration and Blood Glucose Responses after Injections of Regular Insulin and Various Insulin Mixtures, Diabetes Care, 4, 366-376.
12. Van Cauter E., F. Mestrez, J. Sturis, K. S. Polonsky (1992). Estimation of Insulin Secretion Rates from C-peptide Levels, Diabetes, 41, 368-377.
13. Owens D. R., A. Vølund, D. Jones, A. G. Shannon, I. R. Jones, A. J. Birtwell, S. Luzio, S. Williams, J. Dolben, F. N. Creagh, J. R. Peter (1988). Retinopathy in Newly Presenting Non-insulin-dependent (Type 2) Diabetic Patients, Diabetes Research, 9, 59-65.
14. Owens D. R., A. G. Shannon, I. R. Jones, J. Vora, T. M. Hayes, S. Luzio, S. Williams (1986). Metabolic and Hormonal Derangement in Newly Presenting, Previously Untreated Non-insulin Dependent Diabetic Patients, In R. Tattersall (Ed.), Non Insulin Dependent Diabetes Mellitus, Novo, 23-28.
15. Pickup J. C., H. Keen, J. A. Parsons, K. G. M. M. Alberti (1978). Continuous Subcutaneous Insulin Infusion: An Approach to Achieving Normoglycaemia, British Medical Journal, 1(6107), 204-207.
16. Taylor R., P. D. Home, K. G. M. M. Alberti (1981). Plasma Free Insulin Profiles after Administration of Insulin by Jet and Conventional Syringe Injection, Diabetes Care, 4, 377-379.
17. Colagiuri C., J. J. Miller, P. Petocz (1992). Double-blind Crossover Comparison of Human and Porcine Insulins in Patients Reporting Lack of Hypoglycaemia Awareness, The Lancet, 339(8807), 1432-1435.
18. Shannon A. G., S. Colagiuri, J. J. Miller (1990). Comparison of Glycaemic Control with Human and Porcine Insulins – A Meta-analysis, The Medical Journal of Australia, 152, 49.
19. Theodorakis M. J., D. C. Muller, O. Carlson, J. M. Egan (2003). Assessment of Insulin Sensitivity and Secretion Indices from Oral Glucose Tolerance Testing in Subjects with Fasting Euglycemia but Impaired 2-hour Plasma Glucose, Metabolism, 52, 153-1524.
20. Stimmler L., K. Mashiter, G. J. Snodgrass, B. Boucher, M. Abrams (1972). Insulin Disappearance after Intravenous Injection and its Effect on Blood Glucose in Diabetic and Non-diabetic Children and Adults, Clinical Science, 42, 337-344.
21. Kobayashi T., S. Sawano, T. Itoh, K. Kosaka, H. Hirayama, Y. Kasuya (1983). The Pharmacokinetics of Insulin after Continuous Subcutaneous Infusion or Bolus Subcutaneous Injection in Diabetic Patients, Diabetes, 32, 331-336.
22. Kraegen E. W., D. J. Chisholm (1984). Insulin Responses to Varying Profiles of Subcutaneous Insulin Infusion: Kinetic Modelling Studies, Diabetologia, 26, 208-213.
23. Schlichtkrull J. (1977). The Absorption of Insulin, Acta Paediatr Scand, 270, 97-102.
24. Rubenstein A. H., J. L. Clark, F. Melani, D. Steiner (1969). Secretion of Proinsulin C-peptide by Pancreatic Beta Cells and its Circulation in Blood, Nature, 224, 667-669.

25. Polonsky K. S., J. Jaspan, W. Pugh, D. Cohen, M. Schneider, T. Schwartz, A. R. Moossa, H. Tager, A. H. Rubenstein (1983). Metabolism of C-peptide in the Dog: in vivo Demonstration of the Absence of Hepatic Extraction, Journal of Clinical Investigation, 72, 1114-1123.
26. Cobelli C., G. Pacini (1988). Insulin Secretion and Hepatic Extraction in Humans by Minimal Modelling of C-peptide and Insulin Kinetics, Diabetes, 37, 223-231.
27. Vølund A., K. S. Polonsky, R. N. Bergman (1987). Calculated Pattern of Intraportal Insulin Appearance without Independent Assessment of C-peptide Kinetics, Diabetes, 36, 1195-2002.
28. Porte J. R. Jr. A. Pupo (1969). Insulin Response to Glucose: Evidence for a Two Pool System in Man, Journal of Clinical Investigation, 48, 2304-2319.
29. Lang D. A., D. R. Mathews, J. Peto, R. C. Turner (1979). Cyclic Oscillations of Basal Plasma Glucose and Insulin Concentrations in Human Beings, New England Journal of Medicine, 301, 1023-1027.
30. Jones I. R., D. R. Owens, S. Luzio, S. Williams, T. M. Hayes (1989). The Glucose Dependent Insulinotropic Polypeptide Response to Oral Glucose and Mixed Meals is Increased in Patients with Type 2(Non-insulin-dependent) Diabetes Mellitus, Diabetologia, 32, 668-677.
31. Shannon A. G., J. M. Hogg, R. L. Ollerton, S. Luzio, D. R. Owens (1994). A Mathematical Model of Insulin Secretion, IMA Journal of Mathematics Applied in Medicine & Biology, 11, 245-266.
32. Mitchell R., H. Nguyen, B. Thornton, W. Hung, W. Lee, M. Rickard (2004). Mammogram Object Detection using Dendronic Image Analysis, IEEE EMBS Conference, San Francisco, 1763-1765.
33. Hanusse P., P. Guillataud (1992). Dendronic Analysis of Pictures, Fractals and Other Complex Structures, Fractal Geometry and Computer Graphics, Berlin: Springer-Verlag, 203-216.
34. Karssemeijer N. (2002). Detection of Masses in Mammograms. Image Processing Techniques for Tumor Detection, University of Arizona, Tucson, 187-212.
35. Yin F., L. Giger, K. Doi, C. Vyborny, R. Schmidt (1994). Computerized Detection of Masses in Digital Mammograms: Automated Alignment of Breast Images and its Effect on Bilateral-Subtraction Technique, Medical Physics, 21(3), 445-452.
36. Atanassov K. T. (1991). Generalized Nets, World Scientific, Singapore.
37. Atanassov K. T. (1999). Intuitionistic Fuzzy Sets, Physica-Verlag, Heidelberg, New York.
38. Shannon A. G., J. G. Sorsich, K. T. Atanassov (1996). Generalized Nets in Medicine, Prof. Marin Drinov Publishing House of the Bulgarian Academy of Sciences, Sofia.
39. Caden M. J., S. Colagiuri, A. G. Shannon, P. M. Gallagher (1991). Computerized Ambulatory Data Collection for Diabetes Management, Diabetes, Nutrition and Metabolism, 4(1), 93-97.
40. Nguyen H. T., D. Sands, A. Shannon (1994). Fuzzy Logic Control of Plasma Glucose Levels for Insulin Dependent Diabetes, In Patterson B. W. (Ed.) Modeling and Control in Biomedical Systems, International Federation of Automatic Control, Galveston.
41. Skladnev V. N., N. Ghevondian, S. Tarnavskii, N. Paramalingam, T. W. Jones (2010). Clinical Evaluation of a Noninvasive Alarm System for Nocturanl Hypoglycemia, Journal of Diabetes Science and Technology, 4, 67-74.
42. Shannon A. G., R. L. Ollerton, D. R. Owens (1993). A Cholesky Decomposition in Matching Insulin Profiles, In Bergum G. E., A. N. Philippou, A. F. Horadam (Eds.), Applications of Fibonacci Numbers, 5, 497-506.

43. Hung W. T., A. G. Shannon, B. S. Thornton (1994). The Use of a Second Order Recurrence Relation in the Diagnosis of Breast Cancer, The Fibonacci Quarterly, 32, 253-259.
44. Smith G. C. S, J. P. Pell (2003). Parachute Use to Prevent Death and Major Trauma Related to Gravitational Challenge: Systematic Review of Randomised Control Trials, British Medical Journal, 327, 1459-1461.

Prof. Anthony G. (Tony) Shannon, D.Sc., Ph.D., Ed.D.
E-mail: tshannon38@gmail.com; Anthony.Shannon@uts.edu.au

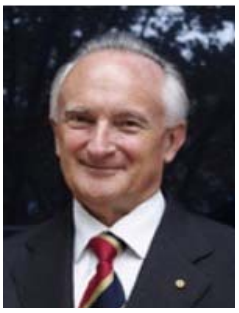

Professor A. G. (Tony) Shannon AM is an Emeritus Professor of the University of Technology, Sydney, (UTS), where he was Foundation Dean of the University Graduate School and Professor of Applied Mathematics, and he is currently working in Health Technologies within the Faculty of Engineering and Information Technology at UTS.

He is co-author of numerous books and articles in medicine, mathematics and education. His research interests are in the philosophy of education and epidemiology, particularly through the application of generalized nets and intuitionistic fuzzy logic. He has taught and mentored at all levels from primary school to post-doctoral where he is still supervising Ph.D. candidates.

Prof. Shannon is a Fellow of several professional societies and a member of several course advisory committees at private higher education providers. He is on the Governing Boards of several approved private higher education providers in Australia. In June 1987 he was appointed a Member of the Order of Australia for services to education. He enjoys reading, walking, theatre, number theory, and thoroughbred racing.

Prof. Hung T. Nguyen, Ph.D.
E-mail: Hung.Nguyen@uts.edu.au

Hung T. Nguyen is a Professor of Electrical Engineering at the University of Technology, Sydney (UTS). He is Dean of the Faculty of Engineering and Information Technology and Director of the Centre for Health Technologies. He received his Ph.D. degree in 1980 from the University of Newcastle, Australia. His research interests include biomedical engineering, advanced control and artificial intelligence. He has developed biomedical devices for diabetes, disability, and cardiovascular diseases. He is a senior member of the Institute of Electrical and Electronic Engineers, a Fellow of the Institution of Engineers, Australia, the British Computer Society and the Australian Computer Society.